

Spin-chain multichannel Kondo model via image impurity boundary condition

Jordan Gaines,¹ Guangjie Li,^{1,2,*} and Jukka I. Väyrynen^{1,†}

¹*Department of Physics and Astronomy, Purdue University, West Lafayette, Indiana 47907, USA.*

²*Department of Physics and Astronomy, University of Utah, Salt Lake City, Utah 84112, USA.*

(Dated: January 15, 2026)

One of the signature observables for the electronic multichannel Kondo model is the impurity entropy, which was found in J_1 - J_2 Heisenberg chains with the open boundary condition (OBC) and periodic boundary condition (PBC), for the one-channel and two-channel cases respectively. However, it is not clear how to generalize OBC and PBC in Heisenberg chains to find the multichannel Kondo impurity entropy with more than two channels. In this paper, we demonstrate that the correct boundary condition for realizing multichannel Kondo physics in Heisenberg chains is the image impurity boundary condition (IIBC) which preserves reflection symmetry and yields the expected impurity entropy, $\ln[(\sqrt{5} + 1)/2]$ for the three-channel case and $\ln\sqrt{3}$ for the four-channel case. Moreover, the IIBC reduces to OBC for the one-channel case and to PBC for the two-channel case. With IIBC, the finite-size scaling of the impurity entropy and the total impurity spin match the finite-temperature corrections in the electronic multichannel Kondo model. Additionally, we show dependence of the impurity entropy, the total impurity spin, and their scaling behaviors on the XXZ anisotropy Δ (equivalently the Luttinger liquid parameter), revealing impurity physics in a multichannel Luttinger liquid.

Introduction. The electronic Kondo effect occurs at low temperatures when conduction electrons screen a magnetic impurity leading to a many-body entangled state [1, 2]. This model was later generalized to consider multiple free-fermion channels overscreening the impurity [3], and this generalization has proved to be a useful model to illustrate exotic many-body phenomena [4–6], especially in mesoscopic devices [7–11], many of which exhibit non-Fermi liquid behavior. A striking example is the zero-temperature impurity entropy $S_{\text{imp}} = \ln g$ where g plays the role of a “ground-state degeneracy” which is generally not an integer [5, 6, 12]. For a Kondo model with M channels, it has been shown through the Bethe Ansatz method [13, 14] and by boundary conformal field theory methods [5, 6, 12, 15, 16] that:

$$g(M) = 2 \cos\left(\frac{\pi}{M+2}\right). \quad (1)$$

Note that $g(M = 1) = 1$ gives zero entropy due to exact screening and $g(M = 2) = \sqrt{2}$ (the quantum dimension of a free Majorana) gives $\ln(2)/2$ entropy due to overscreening [17].

Recently, the multichannel Kondo model has also attracted the attention of the topological quantum computation community since $g(M)$ matches the quantum dimension of various non-Abelian anyons [18, 19], offering the tempting interpretation that an emergent anyon appears at the overscreened impurity. The case of $M = 3$ is of particular interest since $g(M = 3) = \varphi \approx 1.618$, the golden ratio, hints at the existence of Fibonacci anyons [16, 18–21], exotic quasiparticles that may provide a path to universal topological quantum computation [22]. However, the precise connection to anyons remains unclear and, so far, an explicit construction is only known for the Majorana

case $M = 2$ [17, 23], motivating further investigation of $g(M > 2)$ in multichannel Kondo models. Beyond the pure multichannel Kondo models, Ref. [24] explicitly finds the \mathbb{Z}_3 parafermion in the two-impurity Kondo model [11].

While experiments towards observing impurity entropy and verifying Eq. (1) are progressing [25–27], this formula has been numerically verified for up to $M = 4$ channels via various numerical renormalization group (NRG) methods [28–31]. Theoretically, conformal field theory methods, specifically non-abelian bosonization, have shown that the free fermions of the electronic M -channel Kondo model can be bosonized using the “charge” [$U(1)_{2M}$], “spin” [$SU(2)_M$] and “channel” [$SU(M)_2$] currents in the corresponding Kac-Moody algebras [5, 15, 16]. The Kondo interaction is only coupled with the spin sector, suggesting that the fermionic background is not necessary and that Kondo physics can also be studied in systems such as spin chains [32–34] or quantum circuits [35].

Furthermore, it has been widely known that the low-energy effective theory of the spin-chain Heisenberg (XXX) model is described by the $SU(2)_1$ Kac-Moody algebra [36]. Indeed, the one-channel and two-channel Kondo impurity entropies, that is Eq. (1) at $M = 1, 2$, were observed in the open boundary and periodic boundary XXX spin-chain models, respectively [32, 37]. These spin-chain models are of interest because they directly demonstrate that a fermionic background is not necessary to realize Kondo physics. Additionally, the use of a spin-chain model enables us to take advantage of the DMRG algorithm [38], which has seen great success in quantum simulation [39–41]. Spin-chain models also complement fermionic models simulated by NRG. However, as we illustrate below, it is not obvious how to

extend the spin chain formulation to $M > 2$ channels. This extension is one of the key results in this letter and serves to suggest that the physics of the Kondo effects may be bosonic.

Besides the SU(2)-symmetric case, we also consider the effects of exchange anisotropy on the spin-chain multichannel Kondo models. One-channel [42] and two-channel Kondo physics [43] have also been observed in XX Heisenberg chains where the next-nearest neighbor coupling J_2 is not needed, unlike the isotropic case [32, 37]. Notably, the absence of the next-nearest neighbor interaction makes numerical simulation much easier, motivating potential investigation into the viability of XX chains for simulating Kondo physics [44]. Furthermore, one-channel Kondo physics has also been demonstrated for a general anisotropic 1D antiferromagnetic Heisenberg chain [45]. Following these investigations, we introduce anisotropy into our multichannel Kondo model, parametrized by Δ with $\Delta = 1$ being the isotropic model and $\Delta = 0$ being the XX model. We numerically observe that $g \sim d^{(M-1)/2}$ where $d = 1 - \arccos(\Delta)/\pi$ (see Fig. 3). Here, anisotropy is related to the effective Luttinger liquid parameter of the XXZ chain $K = 1/(2d)$ [46], motivating further investigations on the entanglement in multichannel Luttinger liquid impurity models [47–54].

The Multichannel Spin-Chain Kondo Model. We start by introducing our model to realize multichannel Kondo physics using spin chains. We consider a spin-1/2 chain geometry composed of M chains of length L , one chain for each channel, coupled at the left by an impurity spin \mathbf{S}_0 and at the right by an image impurity spin \mathbf{S}'_0 . The spins are coupled via the next-nearest neighbor antiferromagnetic Heisenberg interaction. We will start by considering the isotropic case (XXX model) and then introduce anisotropy later (XXZ model). Concretely, we consider the following Hamiltonian:

$$H = H_{\text{imp}} + H_{\text{image}} + \sum_{k=1}^M H_{\text{bulk}}^k, \quad (2)$$

$$H_{\text{bulk}}^k = J_1 \sum_{j=1}^{L-1} \mathbf{S}_j^k \cdot \mathbf{S}_{j+1}^k + J_2 \sum_{j=1}^{L-2} \mathbf{S}_j^k \cdot \mathbf{S}_{j+2}^k, \quad (3)$$

$$H_{\text{imp}} = J_K \sum_{k=1}^M \left[\mathbf{S}_0 \cdot \left(\mathbf{S}_1^k + \frac{J_2}{J_1} \mathbf{S}_2^k \right) + \frac{J_2}{J_1} \sum_{k' > k} \mathbf{S}_1^k \cdot \mathbf{S}_1^{k'} \right], \quad (4)$$

$$H_{\text{image}} = J'_K \sum_{k=1}^M \left[\mathbf{S}'_0 \cdot \left(\mathbf{S}_L^k + \frac{J_2}{J_1} \mathbf{S}_{L-1}^k \right) + \frac{J_2}{J_1} \sum_{k' > k} \mathbf{S}_L^k \cdot \mathbf{S}_L^{k'} \right], \quad (5)$$

where \mathbf{S}_j^k is the spin-1/2 operator $\mathbf{S} = \hbar(\sigma^x, \sigma^y, \sigma^z)/2$ for the j^{th} spin in k^{th} channel. H_{imp} and H_{image} implement interaction with and across the impurity and image impurity respectively. The nearest-neighbor couplings between spins are also illustrated in Fig. 1(a). For

simplicity, we work in units $J_1 = \hbar = 1$. To implement anisotropy, we use the Hamiltonian Eq. (2) but replace $\mathbf{S}_i \cdot \mathbf{S}_j \rightarrow S_i^x S_j^x + S_i^y S_j^y + \Delta S_i^z S_j^z$. We consider only the critical (gapless) regime $-1 < \Delta \leq 1$ [46]. The isotropic case $\Delta = 1$ gives the multichannel spin-chain Kondo model where the Kondo impurity entropy matches Eq. (1). Note that the $\Delta = 0$ case is a free-fermion model only for $M = 1, 2$, which further demonstrates that the generalization of Fig. 1(a) is nontrivial.

The next-nearest neighbor couplings J_2 are introduced to suppress a marginally irrelevant bulk interaction which contributes to finite size effects [37, 55–58]. These finite size effects are minimized when the marginal coupling constant in the bulk vanishes, which has been shown to occur at the critical point $J_2^c \approx 0.2412$ [57] between the gapless ($J_2 < J_2^c$) and dimerized ($J_2 > J_2^c$) phases. Note further that we fix the chain length L to be even as it has been shown that an odd chain length leads to quantitatively different entanglement entropy profiles which do not match Kondo physics [59–61].

The Subtle $M = 2$ Case. Even the realization of the two-channel model [see Fig. 1(a)] using an $\text{SU}(2)_1$ Heisenberg chain is subtle. Following Ref. [37], we consider a uniform, periodic chain of length $2L+2$ ($J_K = J'_K = J_1$) to extract the impurity entropy at the Kondo intermediate coupling fixed point. The impurity entropy is defined as the difference between the (uniform parts of the) entanglement entropies with and without the impurity, where the entanglement cut at x is sufficiently far from the boundaries [37] [see Fig. 1(a)],

$$S_{\text{imp}}(x) = S_u^{\text{MCK}}(x) - M \cdot S^{\text{OBC}}(x). \quad (6)$$

Here, $S^{\text{OBC}}(x)$ is the von Neumann entanglement entropy of a 1D Heisenberg chain subject to open boundary conditions which is given by the Cardy formula [62]:

$$S^{\text{OBC}}(x) = \frac{c}{6} \ln \left[\frac{2L}{\pi} \sin \left(\frac{\pi x}{L} \right) \right] + \frac{s_1}{2} + \ln g_{\text{Cardy}}, \quad (7)$$

where $c = 1$ is the central charge, s_1 is a non-universal factor, and $g_{\text{Cardy}} = 2^{-1/4}$ is the non-integer ground-state degeneracy associated with a Heisenberg chain [12]. Notably, for the two-channel model ($M = 2$), when $J_K = J_1$, $S_u^{\text{MCK}}(x)$ is given by the Cardy formula for a periodic chain of length $2L+2$ with a cut position $2x+1$ [see Fig. 1(a)],

$$S_u^{\text{MCK}}(x) = S^{\text{PBC}}(x) = \frac{c}{3} \ln \left\{ \frac{2L+2}{\pi} \sin \left[\frac{\pi(2x+1)}{2L+2} \right] \right\} + s_1. \quad (8)$$

When $x \ll L$, the impurity entropy Eq. (6) becomes [37]:

$$S_{\text{imp}}(x) \approx -2 \ln g_{\text{Cardy}} = \ln \sqrt{2}, \quad (M = 2). \quad (9)$$

The value of $g = \sqrt{2}$ coincides with the prediction of Eq. (1) for $M = 2$ and matches the quantum dimension

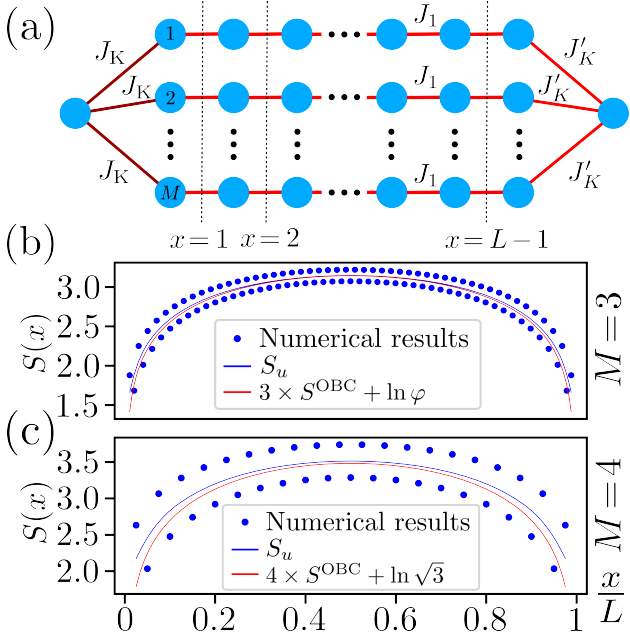


FIG. 1. (a) The geometry of the spin-chain M -channel Kondo model (next-nearest neighbor coupling J_2 not shown). An impurity (left) and an image impurity (right) are both connected to the M bulk channels but with different couplings J_K and J'_K . The nearest-neighbor couplings in the bulk channel are always J_1 . The next nearest-neighbor couplings J_2 are omitted in the figure for simplicity, see Eqs. (3)-(5) for details. The total number of spins is $M \times L + 2$. The cut position is labeled by $x = 1, \dots, L - 1$. The entanglement entropy as a function of x for $J_K = J'_K = J_1$, $J_2 = J_2^c = 0.2412J_1$ obtained from DMRG simulation for (b) $M = 3$ and (c) $M = 4$. The uniform part S_u is close to the prediction $M \times S^{\text{OBC}} + \ln g(M)$ where from Eq. (1) $g(3) = \varphi$ is the golden ratio and $g(4) = \sqrt{3}$. In (b) $L = 100$ and DMRG maximum bond dimension $\chi_{\text{max}} = 4000$ while in (c) $L = 40$ and $\chi_{\text{max}} = 5000$.

of Majorana fermions. That said, it is important to note that $g = \sqrt{2}$ is not unique to the single-impurity two-channel spin-chain Kondo model [43, 63, 64], much less to the two-impurity Kondo model [65, 66].

To go beyond $M = 2$, one needs to first check if generalized models with $M > 2$ channels can give Eq. (1). Unfortunately, a uniform periodic limit employed in Eq. (8) is not known for $M > 2$ channels. Although multichannel spin chain Kondo physics has been studied in Refs. [44, 63, 67–70], it is not clear how to generalize the models to arbitrary number of channels. In this paper, we aim to resolve this ambiguity by proposing a spin-chain geometry to realize Kondo physics for an arbitrary channel number M . To accomplish this task, we introduce the notion of an “image impurity” [71] which reduces to the usual periodic boundary condition when $M = 2$ and the open boundary condition when $M = 1$, see Fig. 1(a). Using our geometry, we are able to realize multichannel Kondo physics using spin

chains for the particularly interesting cases of $M = 3, 4$ channels [Fig. 1(b-c)], obtaining respectively $g \approx 1.623$ and $g \approx 1.787$, close to the predictions $g = \varphi \approx 1.618$ and $g = \sqrt{3} \approx 1.732$ of Eq. (1). We can attribute the differences to a finite-size error, see Fig. 2(a). Finite-size scaling of total impurity spin also confirms that our model realizes MCK physics, see Fig. 2(b).

Numerical Impurity Entropy.

In this work, we use the entanglement entropy as a probe for the M -channel Kondo model. We use DMRG (TenPy [72, 73]) to numerically find the ground state of Eq. (2) and extract the entanglement entropy $S(x)$. The finite system size L induces oscillations in $S(x)$ which allow us to decompose $S(x)$ into a uniform and alternating term [58], $S(x) = S_u(x) + (-1)^x S_a(x)$. In this work, we focus on the uniform part $S_u(x)$ for our analysis of the entanglement structure [32, 37]. Given the entropy profile $S(x)$, we can extract $S_u(x)$ as the average of two cubic fits for the upper blue dots (odd x) and lower blue dots (even x) [59], see Fig. 1(b-c). We then calculate the impurity entropy $S_{\text{imp}}(x)$ as in Eqs. (6)-(7). The case of $J_K = 1$ approximately corresponds to the Kondo fixed point [32, 37] wherein the contribution to the impurity entropy is a consequence of the spin-chain geometry itself.

We first present our numerical values of g for the $M = 3$ and $M = 4$ models. We compute g from $\exp(S_{\text{imp}})$ at $x = L/2$ which corresponds to the closest agreement with Eq. (1) as shown in Fig. 1(b-c). In computing S_{imp} , we also must compute S^{OBC} which requires the determination of the non-universal constant s_1 . Fortunately, s_1 can be easily extracted by comparing DMRG results with Eq. (8) for a periodic XXX chain. Based on this s_1 value, we find that, at the Kondo fixed point ($J_K = 1$), $g \approx 1.623$ for $M = 3$ and $g \approx 1.787$ for $M = 4$. Both these values are very close to the predictions of Eq. (1), i.e., $g(M = 3) = 1.618$ and $g(M = 4) = 1.732$, even for the relatively small system sizes we used. The difference can be attributed to finite size effect as we will discuss below. The bond dimension χ needed is approximately $L^{\alpha c_{\text{eff}}}$ where α is a constant and $c_{\text{eff}} = M$ is the effective central charge. The computational cost is about $\mathcal{O}(L \times \chi^3) \sim \mathcal{O}(L^{3\alpha M+1})$ [72], which scales exponentially with M .

We seek to further support our proposed multichannel model by showing that it reproduces a similar scaling of S_{imp} and ξ_K (Kondo correlation length) [74] observed for the one- and two-channel models [32, 37]. We performed an analysis of S_{imp} as J_K was varied for different values of the system size L to extract ξ_K by fitting to the scaling form $S_{\text{imp}}(x/L, x/\xi_K)$. The extracted ξ_K values are then shown in the inset of Fig. 2(a) where our empirically measured ξ_K indeed appears to scale as e^{a/J_K} . The resulting scaling law for S_{imp} is shown in Fig. 2(a). In contrast to the Fermi-liquid power law $1/(x/\xi_K)$ observed in the spin-chain 1CK model [32, 59, 61] and the non-Fermi liquid power law $\ln(x/\xi_K)/(x/\xi_K)$ for the spin-

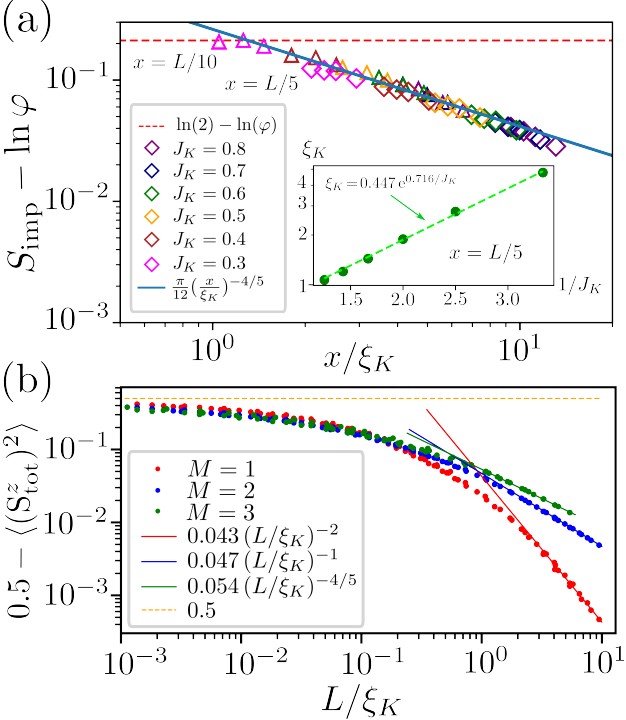


FIG. 2. (a) The impurity entropy scaling plot of the spin-3CK model with $J'_K = 1$ fixed, J_K and total length $L \in [50, 60, 64, 70]$ varying. It shows non-Fermi liquid power law behavior (with power $4/5$) when approaching the predicted impurity entropy $\ln \varphi$ for two cut positions $x = L/5$ and $x = L/10$. (b) The scaling plot for the z -component of total spin of the impurity and the image impurity for spin-1CK (red), 2CK (blue) and 3CK (green) with $J'_K = J_K$. At 1CK, the power law is of Fermi liquid type $1/(L/\xi_K)^2$, but non-Fermi liquid for 2CK and 3CK. Here $\xi_K \sim \exp(2.0/J_K)$. The Kondo couplings $J_K = J'_K \in [0.2, 1]$ and the L values are $[30, 40, 50, 60, 70]$ for $M = 1, 2$ and $[10, 20, 30, 40]$ for $M = 3$.

chain 2CK model [37], we find the non-Fermi liquid power law $1/(x/\xi_K)^{4/5}$ in our spin-chain 3CK model, which is more dominant than the Fermi liquid $1/(x/\xi_K)$ coming from each XXX chain. Both finite-size power laws match the finite-temperature correction to the multichannel impurity entropy [75, 76], which is related to the specific heat [16] when taking the temperature $T \rightarrow 1/(x/\xi_K)$. Fig. 2(a) allows us to estimate the finite-size correction $\exp S_{\text{imp}}(x) - g(M)$. For $M = 3$, $g(3) = \varphi$ and the parameters of Fig. 1(b), we can estimate this correction to be ~ 0.01 for $x = L/2$. Similar estimate for $M = 4$ (albeit using the above ξ_K) gives $\sim 0.03 \equiv \epsilon$, of the same order of magnitude as $S_{\text{imp}} - \ln(\sqrt{3}) = \ln(\sqrt{3} + \epsilon) - \ln(\sqrt{3}) \approx \epsilon/\sqrt{3}$ in Fig. 1(c). Similar to the above finite-size scaling is found for the total impurity spin, discussed next.

Total Impurity Spin. Another signature of MCK physics in our model is exhibited by the total spin of the impurity and image impurity. We first find that the total spin of the whole system is spin 0 for all $0 < J'_K =$

$J_K \leq 1$ and $M = 1, 2, 3$. This singlet formed by the impurity spin and the rest of the spins is similar to the electronic multichannel Kondo model where the impurity spin was connected to entanglement negativity [77]. The negativity was also numerically calculated for the spin-chain 1CK case [78]. We calculate the total spin of the impurity and the image impurity, or equivalently the total spin of the $M \times L$ bulk spins because the whole system has spin 0. Due to the SU(2) symmetry, it is sufficient to calculate the z -component,

$$\langle (S_{\text{tot}}^z)^2 \rangle = \langle (S_0^z + S_0'^z)^2 \rangle = \frac{1}{2} + 2\langle S_0^z S_0'^z \rangle, \quad (10)$$

where $\langle S_0^z S_0'^z \rangle = \langle S_0'^z S_0'^z \rangle = 1/4$ by SU(2) symmetry.

We find that the total impurity spin Eq. (10) depends on the system size and Kondo coupling through the ratio L/ξ_K . The finite-size scaling for $\langle (S_{\text{tot}}^z)^2 \rangle$ is shown in Fig. 2(b). In the $L/\xi_K \rightarrow \infty$ limit, $\langle (S_{\text{tot}}^z)^2 \rangle \rightarrow 1/2$, which corresponds to uncorrelated impurity and image impurity. In the bulk, we get exactly the same value for the z -component total spins, which suggests that two independent spin-1/2 Kondo clouds are formed in the bulk. Because ξ_K is the Kondo-cloud size, we can think of it the following way: One of the Kondo clouds is for the impurity, the other is for the image-impurity and they are decoupled from each other because their sizes ξ_K are very small compared to the chain length L . In this limit, we find $\langle (S_{\text{tot}}^z)^2 \rangle$ to deviate from $1/2$ in a Fermi liquid power law $1/(L/\xi_K)^2$ for $M = 1$ but non-Fermi liquid power laws $1/(L/\xi_K)$ for $M = 2$ and $1/(L/\xi_K)^{4/5}$ for $M = 3$, see Fig. 2(b). These finite-size corrections can be understood to arise in second-order perturbation theory due to the least irrelevant operator with scaling dimension 2 for $M = 1$ and $1 + 2/(M+2)$ for $M \geq 2$ [15, 16]. A similar scaling behavior can be found in Ref. [77] for the negativity of the impurity and the bulk electrons. In the opposite limit $L/\xi_K \rightarrow 0$, the correlation between the impurity and the image-impurity mediated by their Kondo clouds becomes strong. Eventually, the impurity and the image-impurity form a singlet and so do $M \times L$ bulk spins.

Effect of Anisotropy. Due to finite size effects, a next-nearest neighbor coupling J_2 may be needed to suppress a bulk marginal term [32]. In general, J_2^c will be a function of Δ [as will be s_1 in Eq. (7)], which we find numerically [79]. Equipped with these values of $J_2(\Delta)$ and $s_1(\Delta)$, we can then compute the impurity entropy of our multichannel Kondo model, focusing on the uniform case $J_K = 1$. The cases $M = 1, 2$ correspond to open and periodic XXZ Heisenberg chains, where it is known that [80] $g_{\text{cardy}}(\Delta) = [2d(\Delta)]^{-1/4}$ with $d(\Delta) = 1 - \arccos(\Delta)/\pi$ [81], and thus $g(M = 2, \Delta) = \sqrt{2}[d(\Delta)]^{1/2}$. We use DMRG simulations to find $g(M, \Delta)$ for $M = 1, \dots, 4$, shown in Fig. 3(a). We find that $g(M, \Delta) \sim d(\Delta)^\alpha$ closely follows a power law with the exponent $\alpha \approx (M-1)/2$. The prefactor is

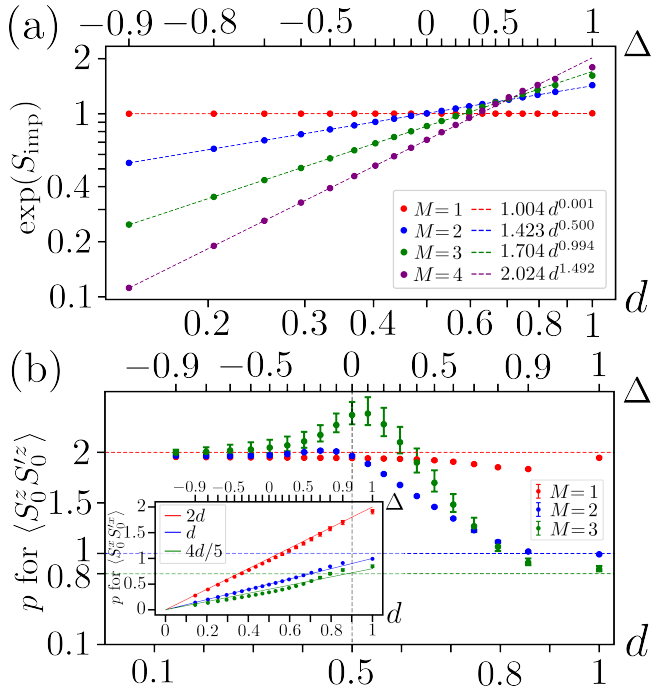


FIG. 3. (a) The effective ground state degeneracy $g = \exp(S_{\text{imp}})$ versus XXZ anisotropy parameter d or Δ for $M = 1, 2, 3, 4$ and $L = 50, 50, 50, 30$ respectively. The power law $g \sim d^{(M-1)/2}$ is observed where the fit lines are for the $\Delta \leq 0$. The fit does not work well near $\Delta = 1$, where it yields $g \sim \sqrt{M}$ instead of Eq. (1). (b) The decay exponent p of the correlation $\langle S_0^z S_0'^z \rangle$ ($\sim 1/L^p$) and $\langle S_0^x S_0'^x \rangle$ (inset) versus d or Δ . The errors are given by the largest and smallest decay exponent fitted using two nearby even L values from 92 to 108 for $M = 1$, 42 to 58 for $M = 2$ and 26 to 42 for $M = 3$.

almost independent of Δ , with only weak dependence near isotropy $d = 1$, where Eq. (1) is recovered.

The power-law behaviors of the S_{imp} in Fig. 2(a) are affected by the XXZ anisotropy [79]. However, in order to better demonstrate the interplay of multichannel Kondo effects and the Luttinger liquid impurity physics [47–54], we show in Fig. 3(b) that the decay exponent p of $\langle S_0^z S_0'^z \rangle \sim 1/L^p$ [equivalent to $\langle S_0^x S_0'^x \rangle$ at $\Delta = 1$ due to SU(2) symmetry, see the inset of Fig. 3(b)] is almost a constant $p(\Delta) = 2$ for $M = 1$ and p transitions from $p = 2$ to $p = 4/(M+2)$ as d goes from 0 to 1 for both the $M = 2, 3$ cases. The $M = 2$ case is exactly the periodic XXZ chain and the dominant decay of $\langle S^z S'^z \rangle$ is $1/L^2$ for $\Delta < 0$ and $1/L^{1/d}$ for $\Delta > 0$ [82]. Currently, there is no analytical analysis on the $M = 3$ case but a similar transition also occurs near $\Delta = 0$, see Fig. 3(a)-(b). The decay exponent of $\langle S_0^x S_0'^x \rangle$ is closely $p(\Delta) = 2d(\Delta)$ for $M = 1$ and $p(M, \Delta) = [4/(M+2)]d(\Delta)$ for both $M = 2$ [80] and $M = 3$. As illustrated above, the exponent $4/(M+2)$ at $\Delta = 1$ is determined by the scaling dimension of the least irrelevant operator $1 + 2/(M+2)$ in multichannel Kondo physics [15, 16]. With anisotropy Δ , all the $M = 1, 2, 3$ exponents are reduced by a factor

$d(\Delta)$.

Summary and Outlook. In summary, we have demonstrated for up to four channels that our proposed spin-chain multichannel Kondo model produces a boundary entropy g consistent with Eq. (1). Thus, a fermionic background is not necessary for observing the multichannel Kondo effect. Therefore, the model can be experimentally realized in quantum computers and simulators [35, 83–92] where the scaling of impurity total spin, Eq. (10), might be a straightforward first step as it requires only two-qubit measurement. Note that our discussion is limited to $J_K \leq 1$ because the model with $J_K > 1$ may enter non-Kondo phases [93].

Our numerical results pose open questions especially for the anisotropic $\Delta \neq 1$ case. Generalizing to multiple channels the Kondo model in a one-channel Luttinger liquid [48, 49, 94–97] (possibly related to quantum Brownian motion [98, 99]) might explain the observations in Fig. 3. Other future directions include exploring possible relation to two-impurity spin-chain Kondo models, extending the model to other quantum impurity models such as non-Hermitian spin-chain multichannel Kondo models [100], and studying finite-temperature and dynamical (finite-frequency) response functions.

Acknowledgments. We have benefited from discussions with A. Zhakenov, A. Tsvelik, C.-M. Jian, E. König, M. Ye, O. Starykh, P. Kattel, R. Wang, T. Sedrakyan, Y. Zhou and Y. Tang. Numerical calculations were performed by using the TeNPy Library [72]. This work was supported by the U.S. Department of Energy, Office of Science, National Quantum Information Science Research Centers, Quantum Science Center. J.G. would like to acknowledge the Office of Undergraduate Research at Purdue University for financial support. He was also financially supported through the Joel Spira Summer Research Award.

* guangjie.li@utah.edu

† vayrynen@purdue.edu

- [1] J. Kondo, Resistance minimum in dilute magnetic alloys, *Progress of Theoretical Physics* **32**, 37 (1964).
- [2] A. C. Hewson, *The Kondo problem to heavy fermions*, Vol. 10031 (Cambridge, UK: Cambridge Univ. Press, 1993) pp. 1–15.
- [3] Nozières, Ph. and Blandin, A., Kondo effect in real metals, *J. Phys. France* **41**, 193 (1980).
- [4] D. L. Cox and A. Zawadowski, Exotic kondo effects in metals: Magnetic ions in a crystalline electric field and tunnelling centres, *Advances in Physics* **47**, 599 (1998).
- [5] A. W. Ludwig, Field theory approach to critical quantum impurity problems and applications to the multi-channel kondo effect, *International Journal of Modern Physics B* **8**, 347 (1994).
- [6] I. Affleck, Quantum impurity problems in condensed matter physics, *Exact Methods in Low-dimensional*

Statistical Physics and Quantum Computing: Lecture Notes of the Les Houches Summer School: Volume 89, July 2008 , 3 (2010).

[7] R. M. Potok, I. G. Rau, H. Shtrikman, Y. Oreg, and D. Goldhaber-Gordon, Observation of the two-channel kondo effect, *Nature* **446**, 167171 (2007).

[8] A. J. Keller, L. Peeters, C. P. Moca, I. Weymann, D. Mahalu, V. Umansky, G. Zarnd, and D. Goldhaber-Gordon, Universal fermi liquid crossover and quantum criticality in a mesoscopic system, *Nature* **526**, 237240 (2015).

[9] Z. Iftikhar, S. Jezouin, A. Anthore, U. Gennser, F. D. Parmentier, A. Cavanna, and F. Pierre, Two-channel kondo effect and renormalization flow with macroscopic quantum charge states, *Nature* **526**, 233236 (2015).

[10] Z. Iftikhar, A. Anthore, A. K. Mitchell, F. D. Parmentier, U. Gennser, A. Ouerghi, A. Cavanna, C. Mora, P. Simon, and F. Pierre, Tunable quantum criticality and super-ballistic transport in a charge kondo circuit, *Science* **360**, 13151320 (2018).

[11] W. Pouse, L. Peeters, C. L. Hsueh, U. Gennser, A. Cavanna, M. A. Kastner, A. K. Mitchell, and D. Goldhaber-Gordon, Quantum simulation of an exotic quantum critical point in a two-site charge kondo circuit, *Nature Physics* **19**, 492499 (2023).

[12] I. Affleck and A. W. W. Ludwig, Universal noninteger “ground-state degeneracy” in critical quantum systems, *Phys. Rev. Lett.* **67**, 161 (1991).

[13] N. Andrei and C. Destri, Solution of the multichannel kondo problem, *Phys. Rev. Lett.* **52**, 364 (1984).

[14] A. M. Tsvelick, The thermodynamics of multichannel kondo problem, *Journal of Physics C: Solid State Physics* **18**, 159 (1985).

[15] I. Affleck, Conformal field theory approach to the kondo effect (1995), arXiv:cond-mat/9512099 [cond-mat].

[16] T. Kimura, Abcd of kondo effect, *Journal of the Physical Society of Japan* **90**, 024708 (2021).

[17] V. J. Emery and S. Kivelson, Mapping of the two-channel kondo problem to a resonant-level model, *Phys. Rev. B* **46**, 10812 (1992).

[18] P. L. S. Lopes, I. Affleck, and E. Sela, Anyons in multichannel kondo systems, *Physical Review B* **101**, 10.1103/physrevb.101.085141 (2020).

[19] Y. Komijani, Isolating kondo anyons for topological quantum computation, *Phys. Rev. B* **101**, 235131 (2020).

[20] C. Han, Z. Iftikhar, Y. Kleeorin, A. Anthore, F. Pierre, Y. Meir, A. K. Mitchell, and E. Sela, Fractional entropy of multichannel kondo systems from conductance-charge relations, *Phys. Rev. Lett.* **128**, 146803 (2022).

[21] T. Ren, E. J. König, and A. M. Tsvelik, Topological quantum computation on a chiral kondo chain, *Phys. Rev. B* **109**, 075145 (2024).

[22] C. Nayak, S. H. Simon, A. Stern, M. Freedman, and S. Das Sarma, Non-abelian anyons and topological quantum computation, *Reviews of Modern Physics* **80**, 10831159 (2008).

[23] A. M. Sengupta and A. Georges, Emery-kivelson solution of the two-channel kondo problem, *Phys. Rev. B* **49**, 10020 (1994).

[24] D. B. Karki, E. Boulat, W. Pouse, D. Goldhaber-Gordon, A. K. Mitchell, and C. Mora, \mathbb{Z}_3 Parafermion in the Double Charge Kondo Model, *Phys. Rev. Lett.* **130**, 146201 (2023).

[25] N. Hartman, C. Olsen, S. Lscher, M. Samani, S. Fallahi, G. C. Gardner, M. Manfra, and J. Folk, Direct entropy measurement in a mesoscopic quantum system, *Nature Physics* **14**, 10831086 (2018).

[26] T. Child, O. Sheekey, S. Lscher, S. Fallahi, G. C. Gardner, M. Manfra, A. Mitchell, E. Sela, Y. Kleeorin, Y. Meir, and J. Folk, Entropy measurement of a strongly coupled quantum dot, *Physical Review Letters* **129**, 10.1103/physrevlett.129.227702 (2022).

[27] C. Han, Z. Iftikhar, Y. Kleeorin, A. Anthore, F. Pierre, Y. Meir, A. K. Mitchell, and E. Sela, Fractional entropy of multichannel kondo systems from conductance-charge relations, *Phys. Rev. Lett.* **128**, 146803 (2022).

[28] A. Weichselbaum, Non-abelian symmetries in tensor networks: A quantum symmetry space approach, *Annals of Physics* **327**, 2972 (2012).

[29] A. K. Mitchell, M. R. Galpin, S. Wilson-Fletcher, D. E. Logan, and R. Bulla, Generalized wilson chain for solving multichannel quantum impurity problems, *Phys. Rev. B* **89**, 121105 (2014).

[30] M. Lotem, E. Sela, and M. Goldstein, Manipulating non-abelian anyons in a chiral multichannel kondo model, *Phys. Rev. Lett.* **129**, 227703 (2022).

[31] M. Lotem, E. Sela, and M. Goldstein, Chiral numerical renormalization group, *Phys. Rev. B* **107**, 155417 (2023).

[32] N. Laflorencie, E. S. Sørensen, and I. Affleck, The kondo effect in spin chains, *Journal of Statistical Mechanics: Theory and Experiment* **2008**, P02007 (2008).

[33] A. E. Nielsen, J. I. Cirac, and G. Sierra, Quantum spin hamiltonians for the $SU(2)_k$ wzw model, *Journal of Statistical Mechanics: Theory and Experiment* **2011**, P11014 (2011).

[34] A. Zhakenov, P. Kattel, A. Gleis, and N. Andrei, in preperation.

[35] S. Sarma, J. I. Väyrynen, and E. J. König, Design and benchmarks for emulating kondo dynamics on a quantum chip, *Phys. Rev. B* **111**, 235142 (2025).

[36] I. Garate and I. Affleck, Interplay between symmetric exchange anisotropy, uniform dzyaloshinskii-moriya interaction, and magnetic fields in the phase diagram of quantum magnets and superconductors, *Phys. Rev. B* **81**, 144419 (2010).

[37] B. Alkurtass, A. Bayat, I. Affleck, S. Bose, H. Johannesson, P. Sodano, E. S. Sørensen, and K. Le Hur, Entanglement structure of the two-channel kondo model, *Phys. Rev. B* **93**, 081106 (2016).

[38] S. R. White, Density matrix formulation for quantum renormalization groups, *Phys. Rev. Lett.* **69**, 2863 (1992).

[39] U. Schollwck, The density-matrix renormalization group in the age of matrix product states, *Annals of Physics* **326**, 96192 (2011).

[40] A. Baiardi and M. Reiher, The density matrix renormalization group in chemistry and molecular physics: Recent developments and new challenges, *The Journal of Chemical Physics* **152**, 10.1063/1.5129672 (2020).

[41] A.-K. Wu, B. Kloss, W. Krinitzin, M. T. Fishman, J. H. Pixley, and E. M. Stoudenmire, Disentangling interacting systems with fermionic gaussian circuits: Application to quantum impurity models, *Phys. Rev. B* **111**, 035119 (2025).

[42] P. Kattel, Y. Tang, J. H. Pixley, and N. Andrei, The

kondo effect in the quantum xx spin chain, *Journal of Physics A: Mathematical and Theoretical* **57**, 265004 (2024).

[43] Y. Tang, P. Kattel, J. H. Pixley, and N. Andrei, Two channel kondo behavior in the quantum xx chain with a boundary defect (2025), arXiv:2501.16415 [cond-mat.str-el].

[44] N. Cramp and A. Trombettoni, Quantum spins on star graphs and the kondo model, *Nuclear Physics B* **871**, 526 (2013).

[45] A. Furusaki and T. Hikihara, Kondo effect in XXZ spin chains, *Phys. Rev. B* **58**, 5529 (1998).

[46] T. Giamarchi, *Quantum physics in one dimension*, Vol. 121 (Clarendon press, 2003).

[47] C. L. Kane and M. P. A. Fisher, Transmission through barriers and resonant tunneling in an interacting one-dimensional electron gas, *Phys. Rev. B* **46**, 15233 (1992).

[48] D. Giuliano, D. Rossini, and A. Trombettoni, From kondo effect to weak-link regime in quantum spin- $\frac{1}{2}$ spin chains, *Phys. Rev. B* **98**, 235164 (2018).

[49] C. Tan, Y. Hang, S. Haas, and H. Saleur, Entanglement flow in the Kane-Fisher quantum impurity problem, *SciPost Phys. Core* **8**, 002 (2025).

[50] P. Kattel, P. R. Pasnoori, J. H. Pixley, and N. Andrei, Edge modes and boundary impurities in the anisotropic heisenberg spin chain, *Phys. Rev. B* **111**, 174430 (2025).

[51] C. Rylands and N. Andrei, Quantum impurity in a luttinger liquid: Exact solution of the kane-fisher model, *Phys. Rev. B* **94**, 115142 (2016).

[52] J. Sirker, S. Fujimoto, N. Laflorencie, S. Eggert, and I. Affleck, Thermodynamics of impurities in the anisotropic heisenberg spin-1/2 chain, *Journal of Statistical Mechanics: Theory and Experiment* **2008**, P02015 (2008).

[53] M. Collura and P. Calabrese, Entanglement evolution across defects in critical anisotropic heisenberg chains, *Journal of Physics A: Mathematical and Theoretical* **46**, 175001 (2013).

[54] J. Zhao, I. Peschel, and X. Wang, Critical entanglement of XXZ Heisenberg chains with defects, *Phys. Rev. B* **73**, 024417 (2006).

[55] K. Nomura and K. Okamoto, Phase Diagram of $S = 1/2$ Antiferromagnetic XXZ Chain with Next-Nearest-Neighbor Interactions, *Journal of the Physical Society of Japan* **62**, 1123 (1993).

[56] K. Nomura and K. Okamoto, Critical properties of $S = 1/2$ antiferromagnetic XXZ chain with next-nearest-neighbour interactions, *Journal of Physics A: Mathematical and General* **27**, 5773 (1994).

[57] S. Eggert, Numerical evidence for multiplicative logarithmic corrections from marginal operators, *Phys. Rev. B* **54**, R9612 (1996).

[58] N. Laflorencie, E. S. Sørensen, M.-S. Chang, and I. Affleck, Boundary effects in the critical scaling of entanglement entropy in 1d systems, *Phys. Rev. Lett.* **96**, 100603 (2006).

[59] E. S. Sørensen, M.-S. Chang, N. Laflorencie, and I. Affleck, Quantum impurity entanglement, *Journal of Statistical Mechanics: Theory and Experiment* **2007**, P08003P08003 (2007).

[60] I. Affleck, N. Laflorencie, and E. S. Sørensen, Entanglement entropy in quantum impurity systems and systems with boundaries, *Journal of Physics A: Mathematical and Theoretical* **42**, 504009 (2009).

[61] E. S. Sørensen, M.-S. Chang, N. Laflorencie, and I. Affleck, Impurity entanglement entropy and the Kondo screening cloud, *Journal of Statistical Mechanics: Theory and Experiment* **2007**, L01001 (2007).

[62] P. Calabrese and J. Cardy, Entanglement entropy and quantum field theory, *Journal of statistical mechanics: theory and experiment* **2004**, P06002 (2004).

[63] A. M. Tsvelik, Majorana fermion realization of a two-channel kondo effect in a junction of three quantum ising chains, *Phys. Rev. Lett.* **110**, 147202 (2013).

[64] A. M. Tsvelik and W.-G. Yin, Possible realization of a multichannel kondo model in a system of magnetic chains, *Phys. Rev. B* **88**, 144401 (2013).

[65] A. K. Mitchell, E. Sela, and D. E. Logan, Two-channel kondo physics in two-impurity kondo models, *Phys. Rev. Lett.* **108**, 086405 (2012).

[66] A. Bayat, Scaling of tripartite entanglement at impurity quantum phase transitions, *Phys. Rev. Lett.* **118**, 036102 (2017).

[67] M. Oshikawa, C. Chamon, and I. Affleck, Junctions of three quantum wires, *Journal of Statistical Mechanics: Theory and Experiment* **2006**, P02008P02008 (2006).

[68] F. Buccheri, R. Egger, R. G. Pereira, and F. B. Ramos, Quantum spin circulator in y junctions of heisenberg chains, *Phys. Rev. B* **97**, 220402 (2018).

[69] F. Buccheri, R. Egger, R. G. Pereira, and F. B. Ramos, Chiral y junction of quantum spin chains, *Nuclear Physics B* **941**, 794 (2019).

[70] D. Giuliano, A. Nava, and P. Sodano, Tunable kondo screening length at a y-junction of three inhomogeneous spin chains, *Nuclear Physics B* **960**, 115192 (2020).

[71] P. Coleman, L. B. Ioffe, and A. M. Tsvelik, Simple formulation of the two-channel kondo model, *Phys. Rev. B* **52**, 6611 (1995).

[72] J. Hauschild and F. Pollmann, Efficient numerical simulations with Tensor Networks: Tensor Network Python (TeNPy), *SciPost Phys. Lect. Notes* , 5 (2018).

[73] The simulation code can be found at <https://purr.purdue.edu/publications/4879/1> or doi:10.4231/JNCZ-WC05 (2025).

[74] A. K. Mitchell, M. Becker, and R. Bulla, Real-space renormalization group flow in quantum impurity systems: Local moment formation and the kondo screening cloud, *Phys. Rev. B* **84**, 115120 (2011).

[75] E. Eriksson and H. Johannesson, Corrections to scaling in entanglement entropy from boundary perturbations, *Journal of Statistical Mechanics: Theory and Experiment* **2011**, P02008 (2011).

[76] E. Eriksson and H. Johannesson, Impurity entanglement entropy in kondo systems from conformal field theory, *Phys. Rev. B* **84**, 041107 (2011).

[77] D. Kim, J. Shim, and H.-S. Sim, Universal thermal entanglement of multichannel kondo effects, *Phys. Rev. Lett.* **127**, 226801 (2021).

[78] A. Bayat, P. Sodano, and S. Bose, Negativity as the entanglement measure to probe the kondo regime in the spin-chain kondo model, *Phys. Rev. B* **81**, 064429 (2010).

[79] See the supplementary material.

[80] I. Affleck, Edge magnetic field in the XXZ spin-chain, *Journal of Physics A: Mathematical and General* **31**, 2761 (1998).

[81] Here $d(\Delta)$ is related to the effective Luttinger liquid parameter $K = 1/(2d)$ [46].

[82] A. O. Gogolin, A. A. Nersesyan, and A. M. Tsvelik, *Bosonization and strongly correlated systems* (Cambridge university press, 2004).

[83] Y. Kim, A. Eddins, S. Anand, K. X. Wei, E. van den Berg, S. Rosenblatt, H. Nayfeh, Y. Wu, M. Zaletel, K. Temme, and A. Kandala, Evidence for the utility of quantum computing before fault tolerance, *Nature (London)* **618**, 500 (2023).

[84] E. Rosenberg, T. I. Andersen, R. Samajdar, A. Petukhov, J. C. Hoke, D. Abanin, A. Bengtsson, I. K. Drozdov, C. Erickson, P. V. Klimov, X. Mi, A. Morvan, M. Neeley, C. Neill, R. Acharya, R. Allen, K. Anderson, M. Ansmann, F. Arute, K. Arya, A. Asfaw, J. Atalaya, J. C. Bardin, A. Bilmes, G. Bortoli, A. Bourassa, J. Bovaard, L. Brill, M. Broughton, B. B. Buckley, D. A. Buell, T. Burger, B. Burkett, N. Bushnell, J. Campero, H.-S. Chang, Z. Chen, B. Chiaro, D. Chik, J. Cogan, R. Collins, P. Conner, W. Courtney, A. L. Crook, B. Curtin, D. M. Debroy, A. D. T. Barba, S. Demura, A. Di Paolo, A. Dunsworth, C. Earle, L. Faoro, E. Farhi, R. Fatemi, V. S. Ferreira, L. F. Burgos, E. Forati, A. G. Fowler, B. Foxen, G. Garcia, J. Genois, W. Giang, C. Gidney, D. Gilboa, M. Giustina, R. Gosula, A. G. Dau, J. A. Gross, S. Habegger, M. C. Hamilton, M. Hansen, M. P. Harrigan, S. D. Harrington, P. Heu, G. Hill, M. R. Hoffmann, S. Hong, T. Huang, A. Huff, W. J. Huggins, L. B. Ioffe, S. V. Isakov, J. Iveland, E. Jeffrey, Z. Jiang, C. Jones, P. Juhas, D. Kafri, T. Khattar, M. Khezri, M. Kieferov, S. Kim, A. Kitaev, A. R. Klots, A. N. Korotkov, F. Kostritsa, J. M. Kreikebaum, D. Landhuis, P. Laptev, K.-M. Lau, L. Laws, J. Lee, K. W. Lee, Y. D. Lensky, B. J. Lester, A. T. Lill, W. Liu, A. Locharla, S. Mandr, O. Martin, S. Martin, J. R. McClean, M. McEwen, S. Meeks, K. C. Miao, A. Mieszala, S. Montazeri, R. Movassagh, W. Mruczkiewicz, A. Nersisyan, M. Newman, J. H. Ng, A. Nguyen, M. Nguyen, M. Y. Niu, T. E. OBrien, S. Omonije, A. Opremcak, R. Potter, L. P. Pryadko, C. Quintana, D. M. Rhodes, C. Rocque, N. C. Rubin, N. Saei, D. Sank, K. Sankaragomathi, K. J. Satzinger, H. F. Schurkus, C. Schuster, M. J. Shearn, A. Shorter, N. Shutty, V. Shvarts, V. Sivak, J. Skruzny, W. C. Smith, R. D. Somma, G. Sterling, D. Strain, M. Szalay, D. Thor, A. Torres, G. Vidal, B. Villalonga, C. V. Heidweiller, T. White, B. W. K. Woo, C. Xing, Z. J. Yao, P. Yeh, J. Yoo, G. Young, A. Zalcman, Y. Zhang, N. Zhu, N. Zobrist, H. Neven, R. Babbush, D. Bacon, S. Boixo, J. Hilton, E. Lucero, A. Megrant, J. Kelly, Y. Chen, V. Smelyanskiy, V. Khemani, S. Gopalakrishnan, T. Prosen, and P. Roushan, Dynamics of magnetization at infinite temperature in a heisenberg spin chain, *Science* **384**, 4853 (2024).

[85] H. Yu, Y. Zhao, and T.-C. Wei, Simulating large-size quantum spin chains on cloud-based superconducting quantum computers, *Phys. Rev. Res.* **5**, 013183 (2023).

[86] T. A. Chowdhury, K. Yu, M. A. Shamim, M. L. Kabir, and R. S. Sufian, Enhancing quantum utility: Simulating large-scale quantum spin chains on superconducting quantum computers, *Phys. Rev. Res.* **6**, 033107 (2024).

[87] S. Trotzky, P. Cheinet, S. Folling, M. Feld, U. Schnorrberger, A. M. Rey, A. Polkovnikov, E. A. Demler, M. D. Lukin, and I. Bloch, Time-resolved observation and control of superexchange interactions with ultracold atoms in optical lattices, *Science* **319**, 295 (2008).

[88] J. Simon, W. S. Bakr, R. Ma, M. E. Tai, P. M. Preiss, and M. Greiner, Quantum simulation of antiferromagnetic spin chains in an optical lattice, *Nature* **472**, 307 (2011).

[89] S. Murmann, F. Deuretzbacher, G. Zürn, J. Bjerlin, S. M. Reimann, L. Santos, T. Lompe, and S. Jochim, Antiferromagnetic heisenberg spin chain of a few cold atoms in a one-dimensional trap, *Phys. Rev. Lett.* **115**, 215301 (2015).

[90] R. Toskovic, R. Van Den Berg, A. Spinelli, I. Eliens, B. Van Den Toorn, B. Bryant, J.-S. Caux, and A. Otte, Atomic spin-chain realization of a model for quantum criticality, *Nature Physics* **12**, 656 (2016).

[91] P. N. Jepsen, J. Amato-Grill, I. Dimitrova, W. W. Ho, E. Demler, and W. Ketterle, Spin transport in a tunable heisenberg model realized with ultracold atoms, *Nature* **588**, 403 (2020).

[92] C. J. van Diepen, T.-K. Hsiao, U. Mukhopadhyay, C. Reichl, W. Wegscheider, and L. M. K. Vandersypen, Quantum simulation of antiferromagnetic heisenberg chain with gate-defined quantum dots, *Phys. Rev. X* **11**, 041025 (2021).

[93] P. Kattel, P. R. Pasnoori, J. H. Pixley, P. Azaria, and N. Andrei, Kondo effect in the isotropic heisenberg spin chain, *Phys. Rev. B* **109**, 174416 (2024).

[94] D.-H. Lee and J. Toner, Kondo effect in a luttinger liquid, *Phys. Rev. Lett.* **69**, 3378 (1992).

[95] A. Furusaki and N. Nagaosa, Kondo effect in a tomonaga-luttinger liquid, *Phys. Rev. Lett.* **72**, 892 (1994).

[96] J. Maciejko, C. Liu, Y. Oreg, X.-L. Qi, C. Wu, and S.-C. Zhang, Kondo effect in the helical edge liquid of the quantum spin hall state, *Phys. Rev. Lett.* **102**, 256803 (2009).

[97] J. I. Väyrynen, F. Geissler, and L. I. Glazman, Magnetic moments in a helical edge can make weak correlations seem strong, *Phys. Rev. B* **93**, 241301 (2016).

[98] H. Yi and C. L. Kane, Quantum brownian motion in a periodic potential and the multichannel kondo problem, *Phys. Rev. B* **57**, R5579 (1998).

[99] H. Yi, Resonant tunneling and the multichannel kondo problem: Quantum brownian motion description, *Phys. Rev. B* **65**, 195101 (2002).

[100] P. C. Burke and A. K. Mitchell, Non-hermitian numerical renormalization group: Solution of the non-hermitian kondo model (2025), arXiv:2504.07019 [cond-mat.str-el].

Supplementary materials on
“Spin-chain multichannel Kondo model via image impurity boundary condition”

Jordan Gaines¹, Guangjie Li^{1,2}, Jukka I. Väyrynen¹,

¹ Department of Physics and Astronomy, Purdue University, West Lafayette, Indiana 47907, USA

² Department of Physics and Astronomy, University of Utah, Salt Lake City, Utah 84112, USA

These supplementary materials contain details about $J_2(\Delta)$ and $s_1(\Delta)$ in Sec. S1 and the 3CK $g(\Delta)$ values for all $J_2 = 0$ in Sec. S2. Finally, we investigate the influence of anisotropy Δ on the impurity entropy scaling in Sec. S3, and in Sec. S4 we evaluate spin-spin correlation functions between the impurity and bulk spins.

S1. THE CRITICAL J_2 FOR $\Delta \neq 1$

To adequately study Kondo physics when $\Delta \neq 1$, we will need to determine empirical values for $J_2^c(\Delta)$. By numerically comparing the entanglement entropy of the XXZ chain with different values of J_2^c to Eq. (7), we can find the J_2^c value that most closely reproduces g_{Cardy} and hence obtain a good estimate of J_2^c . For each J_2^c , we also need to repeat our prescription for finding s_1 which will now also be a function of Δ . The resulting J_2^c values are shown in Fig. S1 below. Note that these critical values $J_2^c(\Delta)$ are different from the dimer-fluid critical points [55] and the Gaussian fixed points [56] of the XXZ chain.

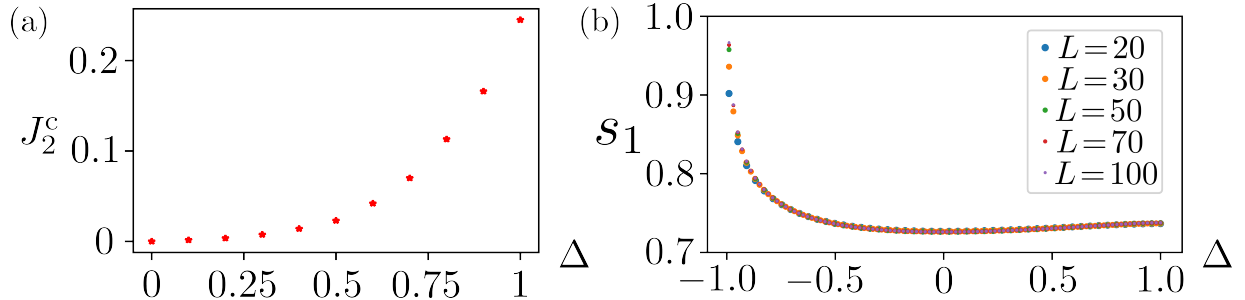


FIG. S1. (a) J_2^c v.s. anisotropy Δ for $\Delta > 0$. When $\Delta \leq 0$, we use $J_2^c = 0$. (b) s_1 v.s. anisotropy Δ for $L = 20, 30, 50, 70, 100$ and $J_2 = 0$.

S2. THE MEASURED 3CK g FOR ALL $J_2 = 0$

In this section, we compare the 3CK anisotropy results using $J_2 = J_2^c(\Delta)$ with the same parameters except $J_2 = 0$ for all Δ and $L = 20, 50, 70$. We observe that for the multichannel spin chain Kondo model the next-nearest neighbor coupling J_2 does not play a crucial role, see Fig. S2.

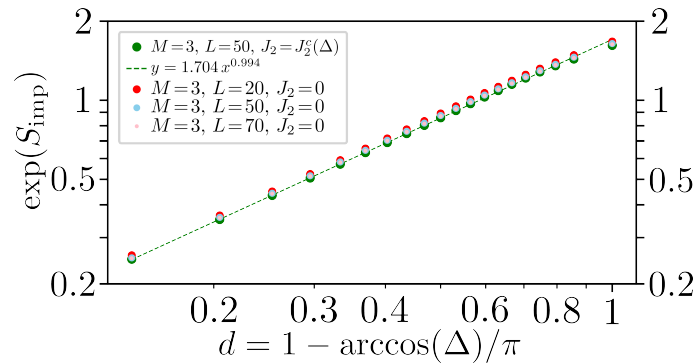


FIG. S2. The results with $J_2 = J_2^c(\Delta)$ and $J_2 = 0$ are very close. The green points and dashed line have been shown in Fig. 3.

S3. THE $S_{\text{imp}} - \ln(g)$ POWER LAW V.S. ANISOTROPY Δ

We calculated the $S_{\text{imp}}(x)$ with $x = L/4$ by taking $\Delta \in [-0.9, -0.8, \dots, 1]$ and $L \in [44, 48, 52, 56]$ for $M = 1, 2$ and $L \in [28, 32, 36, 40]$ for $M = 3$. By fitting the data we obtained, we get the exponent p in $S_{\text{imp}} - \ln[g(M, \Delta)] \sim 1/L^p$ where $g(1, \Delta) = 1$, $g(2, \Delta) = \sqrt{2}d^{1/2}$ and $g(3, \Delta) = \frac{\sqrt{5}+1}{2}d(\Delta)$ with $d(\Delta) = 1 - \arccos(\Delta)/\pi$. The $\Delta = 1$ results for

$M = 1, 3$ in the following Fig. S3 match the expected exponent 1 for $M = 1$ and $4/5$ for $M = 3$. The $M = 2, \Delta = 1$ behavior is $\ln(L)/L$, not the power law $1/L$ and thus a lower effective power-law scaling ~ 0.6 is observed. We did not find any simple dependence on d and Δ for the exponent p , not like what we found in Fig. 3(b) for the correlation functions.

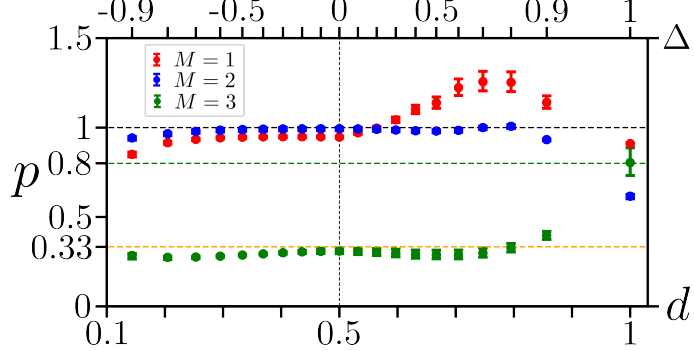


FIG. S3. The scaling exponent p for $S_{\text{imp}} - \ln(g) \sim 1/L^p$ versus anisotropy parameter d or Δ with $J_2 = J_2^c(\Delta)$ for $M = 1, 2, 3$.

S4. THE $\langle S_0^x S_r^{k=1,x} \rangle$ POWER LAW FOR DIFFERENT ANISOTROPY PARAMETERS

In order to show the Luttinger liquid physics, we also calculate the correlation functions between the impurity spin S_0 and the spin in the k th channel and at position $r = 1, \dots, L, L + 1$ where $r = L + 1$ denotes image-impurity. For example, the x-component can be written as $\langle S_0^x S_r^{k=1,x} \rangle = \langle S_0^x S_r^{k=1,x} \rangle_U + (-1)^r \langle S_0^x S_r^{k=1,x} \rangle_A$ as a function of r and the alternating part $\langle S_0^x S_r^{k=1,x} \rangle_A$ is shown in Fig. S4. The $M = 2$ case (periodic XXZ chain) matches with the prediction in Ref. [80].

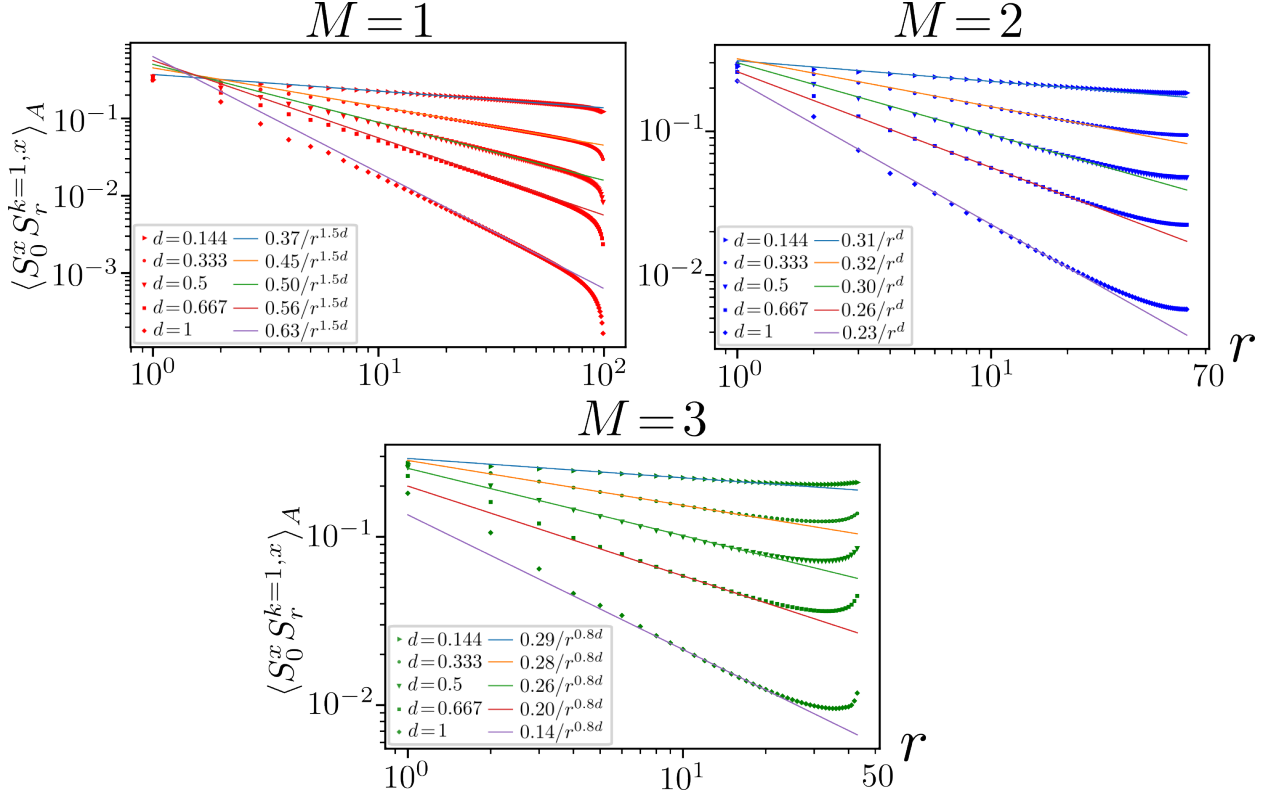


FIG. S4. A log-log plot of $\langle S_0^x S_r^{k=1,x} \rangle_A$ v.s. r for $M = 1, 2, 3$ (red, blue, green) and $L = 98, 58, 42$ respectively. The Luttinger-liquid scaling behavior is clearly seen from the power-law lines with exponents $(3/2)d, d, (4/5)d$ for $M = 1, 2, 3$ and the Luttinger parameter is $K = 1/(2d)$.